

A Synaptic Mechanism for Temporal Filtering of Visual Signals

Article (Published Version)

Baden, Tom, Nikolaev, Anton, Esposti, Federico, Dreosti, Elena, Odermatt, Benjamin and Lagnado, Leon (2014) A Synaptic Mechanism for Temporal Filtering of Visual Signals. *PLoS Biology*, 12 (10). e1001972. ISSN 1544-9173

This version is available from Sussex Research Online: <http://sro.sussex.ac.uk/id/eprint/68928/>

This document is made available in accordance with publisher policies and may differ from the published version or from the version of record. If you wish to cite this item you are advised to consult the publisher's version. Please see the URL above for details on accessing the published version.

Copyright and reuse:

Sussex Research Online is a digital repository of the research output of the University.

Copyright and all moral rights to the version of the paper presented here belong to the individual author(s) and/or other copyright owners. To the extent reasonable and practicable, the material made available in SRO has been checked for eligibility before being made available.

Copies of full text items generally can be reproduced, displayed or performed and given to third parties in any format or medium for personal research or study, educational, or not-for-profit purposes without prior permission or charge, provided that the authors, title and full bibliographic details are credited, a hyperlink and/or URL is given for the original metadata page and the content is not changed in any way.



A Synaptic Mechanism for Temporal Filtering of Visual Signals

Tom Baden^{1,9}, Anton Nikolaev^{1,9}, Federico Esposti¹, Elena Dreosti¹, Benjamin Odermatt¹, Leon Lagnado^{1,2*}

1 MRC Laboratory of Molecular Biology, Neurobiology Division, Cambridge, United Kingdom, **2** School of Life Sciences, University of Sussex, Brighton, United Kingdom

Abstract

The visual system transmits information about fast and slow changes in light intensity through separate neural pathways. We used *in vivo* imaging to investigate how bipolar cells transmit these signals to the inner retina. We found that the volume of the synaptic terminal is an intrinsic property that contributes to different temporal filters. Individual cells transmit through multiple terminals varying in size, but smaller terminals generate faster and larger calcium transients to trigger vesicle release with higher initial gain, followed by more profound adaptation. Smaller terminals transmitted higher stimulus frequencies more effectively. Modeling global calcium dynamics triggering vesicle release indicated that variations in the volume of presynaptic compartments contribute directly to all these differences in response dynamics. These results indicate how one neuron can transmit different temporal components in the visual signal through synaptic terminals of varying geometries with different adaptational properties.

Citation: Baden T, Nikolaev A, Esposti F, Dreosti E, Odermatt B, et al. (2014) A Synaptic Mechanism for Temporal Filtering of Visual Signals. PLoS Biol 12(10): e1001972. doi:10.1371/journal.pbio.1001972

Academic Editor: Stephen A. Baccus, Stanford University School of Medicine, United States of America

Received: May 2, 2014; **Accepted:** September 10, 2014; **Published:** October 21, 2014

Copyright: © 2014 Baden et al. This is an open-access article distributed under the terms of the Creative Commons Attribution License, which permits unrestricted use, distribution, and reproduction in any medium, provided the original author and source are credited.

Data Availability: The authors confirm that all data underlying the findings are fully available without restriction. All relevant data are within the paper and its Supporting Information files.

Funding: Wellcome Trust (083220). Medical Research Council, UK (MRC-LMB; no grant number applicable). The funders had no role in study design, data collection and analysis, decision to publish, or preparation of the manuscript.

Competing Interests: The authors have declared that no competing interests exist.

Abbreviations: AI, adaptation index; BC, bipolar cell; DC, direct current; dpf, days post fertilization; EGFP, enhanced green fluorescent protein; IP, intermediate pool; IPL, inner plexiform layer; OGB, Oregon green BAPTA; RGC, retinal ganglion cell; ROI, region of interest; RP, reserve pool; RRP, readily releasable pool.

* Email: L.Lagnado@sussex.ac.uk

⁹ These authors contributed equally to this work.

Introduction

The retina analyzes the visual world through a series of spatio-temporal filters that establish parallel representations for transmission to the brain [1–4]. The anatomical organization of these channels is established in the inner plexiform layer (IPL), which is organized into five to six distinct strata containing the dendrites of as many as 20 different types of retinal ganglion cell (RGC) [2]. In each stratum, bipolar cells (BCs) with distinct filtering properties make excitatory synaptic connections with defined subsets of RGCs [5]. For instance, “transient” RGCs are thought to receive excitatory inputs from BCs with bandpass characteristics, while “sustained” RGCs receive inputs from BCs acting as low-pass filters [6].

A long-standing question is how multiple spatio-temporal filters are built using the limited numbers of neurons responding to a particular region of the visual field [7–9]. An answer might lie in reconsidering the fundamental neural element through which the visual signal is transmitted to the inner retina: although individual BCs have diverse properties, their output is transmitted through a much more numerous and heterogeneous component of neural circuits—synapses [10]. Indeed, recent evidence indicates that different synapses of the same BC transmit the visual signal with varying kinetics because of local interactions with different types of inhibitory amacrine cells [11]. Here we ask whether heterogeneous

transmission of the visual signal might also reflect intrinsic variations between the various synaptic compartments of a BC. The property we concentrate on is the volume of the terminal, which is expected to influence the amplitude and kinetics of the presynaptic calcium signal controlling neurotransmission [12].

To observe the activity of multiple BC synapses we used zebrafish expressing fluorescent proteins reporting the fusion of synaptic vesicles or the presynaptic calcium signal driving fusion [13,14]. Here we demonstrate that BC terminals of different sizes tend to transform the visual signal in different ways. On average, smaller terminals generate calcium transients that are larger and faster, resulting in a higher initial gain of responses to an increase in temporal contrast followed by more profound adaptation. Small terminals also transmit high frequencies more effectively. Such differences in the outputs of small and large terminals are also observed in individual cells, which therefore have an intrinsic ability to filter visual information through channels with different gains, temporal filters and adaptive properties.

Results

The Volume of Bipolar Cell Terminals Determines the Gain and Kinetics of Signal Transmission

In the vertebrate retina, signals from rod and cone photoreceptors travel through BCs to be transmitted through synaptic

Author Summary

The process of neurotransmission involves the conversion of electrical signals into the release of a chemical neurotransmitter from the neurons synaptic terminal, and the key trigger for this release is a rise in calcium concentration. Accordingly, the amplitude and speed of this calcium signal controls the amplitude and time-course of synaptic communication. Working on the synaptic terminals of fish retinal bipolar cells, we show that the presynaptic calcium signal and the subsequent neurotransmitter release are shaped by the basic property of synapse volume. Using a combination of experimental approaches and computational models, we found that large synapses are slow and adapt little during ongoing stimulation, while small synapses are fast and show more profound adaptation. This observation leads to a second key concept: since neurons usually have several presynaptic terminals that may vary in volume, a single neuron can, in principle, forward different synaptic signals to different postsynaptic partners. We provide direct evidence that this is the case for bipolar cells of the fish retina.

terminals of various sizes (Figure 1A). To survey the activity of many BC synapses in a live animal, we imaged eight to ten days post fertilisation (dpf) zebrafish larvae expressing *sypHy*, a reporter of vesicle fusion (Figure 1B) [14,15], or *SyGCaMP2*, which signals the presynaptic calcium transient [13,16]. Regions of interest defining individual terminals in images of the IPL were generated using an algorithm based on a Laplace operator (Figure 1B) [17], from which we estimated the “effective terminal radius” (Materials and Methods). A survey of 5,061 terminals revealed a wide variation in radius with a mean of $1.13 \pm 0.40 \mu\text{m}$ (Figure 1C, black bars). Terminals of different sizes were not distributed randomly through the IPL (Figures 1D and S1I): terminals in layers 2 and 6 were significantly larger than the average across the whole population of BCs, while terminals in layers 1, 3, 4, and 5 were significantly smaller.

How do these variations in the volume of the presynaptic compartment affect the calcium signal that is generated when a stimulus alters the membrane potential and the rate of calcium influx? To investigate this question we imaged *SyGCaMP2* and measured the average response over the whole region of interest (ROI) defining each terminal. Although this procedure will neglect calcium gradients within the terminal, these gradients will not be maintained when calcium influx is modulated at frequencies relevant to vision (see below). In a sample of 932 ON terminals, the initial rate of rise of the calcium signal elicited by a full field step of light was approximately twice as fast in the smallest terminals compared to the largest, and the calcium concentration reached a higher steady-state level (Figure 1E_{1,2}). Variations in terminal size were also correlated with differences in the kinetics of exocytosis, as measured in fish expressing *sypHy*. In a sample of 438 ON terminals, the relative rate of vesicle release in response to the same stimulus (quantified as a percentage of vesicles released per second) varied by a factor of at least two between the smallest and largest terminals (Figure 1F_{1,2}) [14,18]. A similar relationship between release amplitude and terminal size was observed in the OFF channel (Figure S1G).

A correlation between the size of a terminal and the amplitude of its response was also observed when the temporal contrast of the stimulus was increased while keeping the mean luminance constant. Figure 1G₁ shows averaged *SyGCaMP2* responses to modulation of light intensity at 1 Hz (100% contrast). The power

of the calcium signal at the fundamental frequency was greater in small terminals ($r = 0.6\text{--}1.3 \mu\text{m}$) than in large ($r = 2.1\text{--}4.1 \mu\text{m}$), varying by a factor of at least three across the population (Figure 1G₂).

Does the correlation between the size of the terminal compartment and the release rate reflect the network in which the terminal is embedded? For instance, one scenario might be that large terminals respond with lower gain because they receive stronger inhibitory feedback from amacrine cells. To test this possibility, we blocked GABAergic inhibition through ionotropic receptors by injecting 100 μM picrotoxin into the eye (Figure 2). This manipulation increased the amplitude of the exocytic response across terminals of all sizes, as would be expected when feedback inhibition is reduced [18,19], but larger terminals continued to respond with lower gain. This observation suggests that the correlation between terminal size and release rate reflects intrinsic properties of the terminal rather than the influence of the network it is embedded in.

Might the correlation between stimulus-dependent changes in the brightness of terminals and estimates of their size be caused by a bias in the detection algorithm, perhaps causing smaller terminals to be detected only when their fluorescence signal was strong enough? Two lines of evidence indicated that this was not the case. First, the distribution of terminal sizes was very similar when measured in transgenic fish expressing synaptophysin-enhanced green fluorescent protein (EGFP), a fluorescent marker of synapses that is not affected by neural activity (Figure 1C, red bars). Second, estimates of terminal size did not differ significantly when measurements were compared under conditions of high and low activity, as described in Figure S1 (See Methods). The results in Figure 1 therefore indicate that the volume of the presynaptic compartment is closely linked to the gain with which BCs transmit the visual signal to the inner retina.

Different Calcium Dynamics in Small and Large Terminals of Individual Bipolar Cells

Are differences in gain maintained in small and large terminals of the same cell? We investigated this question both *in vivo* and *in vitro*. *In vivo* experiments used zebrafish transiently expressing *Ribeye::GCaMP5* in sparse populations of BCs. Square-wave stimuli (100% contrast) were presented at various frequencies, and Figure 3A–3C shows results from one BC responding to a 1 Hz stimulus. The calcium signal in the smaller of the two terminals clearly exhibited the larger degree of modulation (Figure 3B; cf. Figure 1G₁), and the power of the response peaked at a higher frequency (Figure 3C). Qualitatively similar results were obtained from four BCs.

We next used slices of goldfish retina to make whole-cell recordings directly from the large terminal of “mixed” BCs, which is connected to smaller presynaptic compartments by narrow processes. Introduction of the Ca^{2+} indicator Oregon green BAPTA (OGB-5N) allowed us to compare presynaptic calcium signals in the large and small compartments while achieving direct electrical control of the terminal system (Figure 3D; cf. Figure 1A) [20]. A BC generating a graded voltage response is shown in Figure 3E. The OGB-5N signal in the smaller terminal (red) rose faster than that in the large (black), reached more than double the concentration, and then decayed more rapidly. Similar results were observed in eight cells generating purely graded responses.

Many BCs in the retina of fish generate voltage spikes as well as graded responses [16,21,22], and terminal volume also affected the presynaptic calcium transient generated by these electrical responses [16,21–23]. In the example in Figure 3F, the small terminal (red) responded to each spike with a clear Ca^{2+} transient,

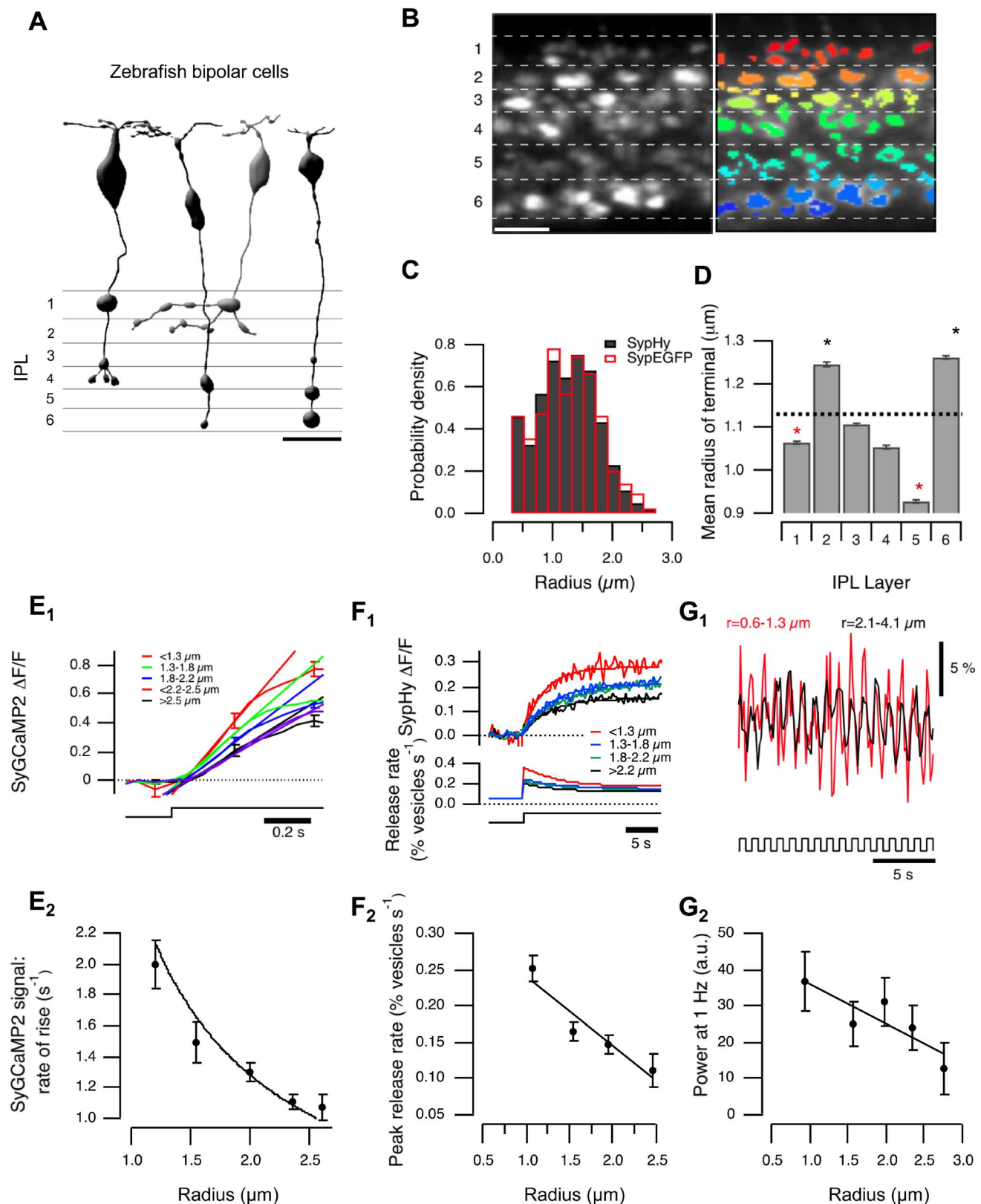


Figure 1. Variations in terminal size, calcium signals, and vesicle release. (A) BCs transmit through multiple terminals. Left: published examples of zebrafish cone BCs [64] illustrate the range of presynaptic terminal sizes. Scalebar = 10 μm . (B) BC terminals in the IPL of a zebrafish (10 dpf) expressing SyHy under control of the *ribeye* promoter. Left: Raw image showing six strata of the IPL. Right: Overlay of ROIs defining terminals.

Scale bar = 10 μm . (C) The distribution of the effective terminal radii. Black bars show estimates obtained in fish expressing syHy ($n=5,061$ terminals from seven fish), and the red bars shows the distribution measured in fish expressing synaptophysin-EGFP ($n=421$ terminals from one fish). Distribution of sizes calculated with SyGCaMP2 is shown in Figure S1H. (D) Variations in average radius of terminals in each stratum. The average radius over the whole IPL was $1.13 \pm 0.40 \mu\text{m}$ (dashed line). Stars mark strata in which the average radius was significantly greater or smaller ($p < 0.001$, Wilcoxon rank-sum test, n varies between 560 and 930 terminals). Similar distributions calculated for individual layers are shown in Figure S1I. (E) Relation between terminal size and calcium signals. (E₁) SyGCaMP2 signals in response to a step of light ($\lambda = 590 \text{ nm}$; for details see methods) in ON terminals, averaged over groups of the effective radius shown ($n=143, 347, 286, 114$, and 36 , respectively). Straight lines fitted over the initial phase. Significant difference between groups 1, 3, and 5 (Student's t test: $p_{(1-3)} = 0.004$; $p_{(3-5)} = 0.005$; $p_{(1-5)} < 0.001$). (E₂) The rate of rise of the SyGCaMP2 signal varies as the inverse of the radius, as shown by the fitted curve ($n=926$ from five fish). Spearman correlation coefficient = -1 , critical value ($p=0.05$) = 0.85 . (F) Relation between terminal size and peak rate of vesicle release. (F₁) SyHy signals in response to a step of light in ON terminals, averaged over groups of the effective radius shown ($n=117, 176, 113$, and 33 terminals from five fish). The lower panel shows the conversion into relative release rates, as described [14]. (F₂) The initial rate of vesicle release as a function of radius (total $n=438$ terminals from five fish). The points fall on a line. Spearman correlation = -1 , critical value ($p=0.05$) = 0.9 . (G) terminal size and modulation of presynaptic calcium. (G₁) SyGCaMP2 signal driven by modulation of light intensity at 1 Hz (100% contrast, square wave). Red trace averaged over OFF contrast responding terminals with $r=0.6$ – $1.3 \mu\text{m}$; black trace averaged over OFF contrast responding terminals with $r=2.1$ – $4.1 \mu\text{m}$. (G₂) relative power of the signal at 1 Hz as a function of radius ($n=98, 89, 68, 37$, and 9 terminals from four fish). Points were fitted with a line. Responses to light decrements are shown in Figure S1G. doi:10.1371/journal.pbio.1001972.g001

but the signal in the large terminal (black) was smaller and slower, and the response to a train of spikes was dominated by the gradual accumulation of Ca^{2+} . Figures 3G–3I summarize these properties in 16 pairs of terminals (eight graded and eight spiking), each pair from a different BC. In all cases, global Ca^{2+} signals were faster and larger in the smaller of two connected terminals. The same observation was made when the patch-pipette was placed on the soma (Figure S3). The results in Figure 3 demonstrate that variations in terminal volume profoundly affected the activity of different synapses providing the output from a single BC.

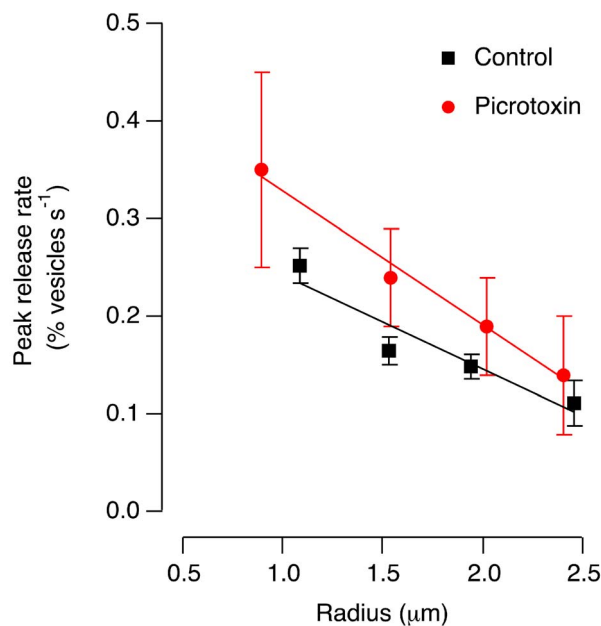


Figure 2. The relation between terminal volume and release rate persists when GABAergic feedback inhibition is blocked. The initial rate of release in response to a step of light in control terminals (black, from Figure 1F₂) is compared with measurements in which 100 M picrotoxin was injected in the front of the eye (77 ON terminals from three fish). The line fitted to the control has a slope of -0.096 ± 0.023 , and the line fitted to the picrotoxin measurements has a slope of -0.138 ± 0.01 dependence peak release size (Figure 1F₂). Note that picrotoxin also increased the amplitude of the exocytic response, as would be expected when feedback inhibition is reduced. doi:10.1371/journal.pbio.1001972.g002

The Relation between the Decay of the Calcium Transient and the Radius of the Terminal

The time-constant of decay of a calcium transient (τ_{decay}) was directly proportional to the radius of the terminal (r), as shown Figure 3J. This observation was made both when r was estimated from images of terminals filled with dye, and when r was calculated from the capacitance of terminals detached from the cell body. This simple linear relation is notable because it is predicted by single compartment models of calcium dynamics in which there are no significant calcium gradients [24,25]. The appropriateness of a single compartment model for BC terminals can be understood in terms of the characteristic time, t_{eq} , with which a calcium gradient collapses in a volume of radius r after calcium influx ceases:

$$t_{\text{eq}} \approx \frac{r^2}{6D_{\text{Ca}}}$$

where D_{Ca} is the diffusion coefficient of calcium [26]. Assuming $D_{\text{Ca}} = 220 \mu\text{m}^2/\text{s}$ [27], t_{eq} is only $\sim 0.75 \text{ ms}$ in a terminal of $r = 1 \mu\text{m}$, indicating that a calcium gradient will collapse on a much shorter time-scale than stimuli relevant to vision. Even in the largest terminals with $r = 5 \mu\text{m}$, t_{eq} is $\sim 19 \text{ ms}$, which is less than half the period of a stimulus fluctuating at 20 Hz. The lack of any appreciable calcium gradients on these time-scales was confirmed in a 3-D model in which calcium influx occurred through clusters of calcium channels (Figure S3). Calcium signals on these spatial scales have been demonstrated to trigger neurotransmitter release from ribbon synapses of fish bipolar cells, although calcium nanodomains very close to calcium channels also play a role in ribbon-type synapses in other neurons and other species [28].

These considerations indicate that there is a direct and causal link between the volume of the presynaptic compartment and the amplitude and kinetics of the calcium transient caused by a stimulus. But why is the volume of the presynaptic compartment also correlated with its output measured as vesicle release (Figure 1F)? Such a link is expected, because it is the calcium signal in the terminal that drives the output.

A Single-Compartment Model of Presynaptic Calcium Dynamics

To explore how variations in the size of BC terminals might impact on transmission of visual signals we modeled this process in two stages, described in detail in Text S1. The output from the first stage was the dynamics of calcium in the terminal, and is shown schematically in Figure 4A. The second stage used these calcium

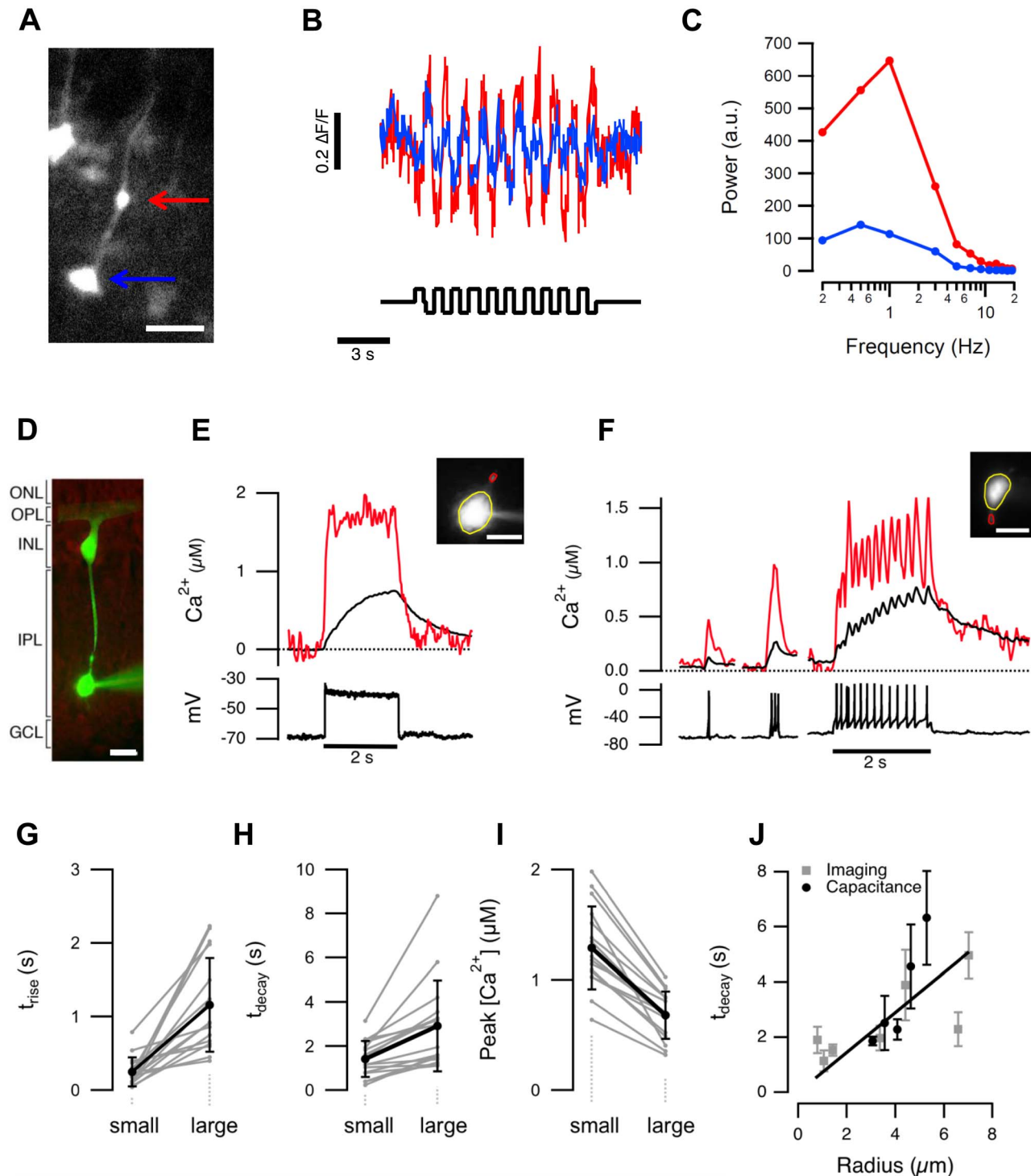


Figure 3. Different calcium signals in small and large terminals of the same cell. (A) A BC expressing GCaMP5. Large and small terminals are indicated by the blue and red arrows. Scalebar 10 μm . (B) Responses of the terminals in (A) to a stimulus modulated at 1 Hz. (C) Power spectrum of the responses from large and small terminals calculated for different stimulus frequencies. (D) Mixed BC filled with OGB-5N in a slice of goldfish retina. Scale bar 10 μm . (E) Spatially averaged Ca^{2+} signals in the small (red) and large (black) terminal during a 2 s depolarizing current step (10 pA). This BC did not generate spikes. (F) A comparison of Ca^{2+} signals in the small and large terminal of a "spiking" BC. Each spike caused a calcium transient that was larger and faster in the smaller terminal. (G–I) Time constants of the calcium signal rise (t_{rise}), decay (t_{decay}), and peak amplitude, evaluated in 16 pairs of small and large terminals. For small and large, $t_{\text{rise}} = 0.25 \pm 0.20$ and 1.16 ± 0.64 s; $t_{\text{decay}} = 1.42 \pm 0.82$ and 2.91 ± 2.05 s; amplitude = 1.29 ± 0.38 and 0.68 ± 0.21 μM . All these parameters were significantly different in small and large terminals ($p < 0.001$; Wilcoxon ranked sum, $n = 16$ cells from nine adult retinæ). The average radii of the small and large terminals were 1.1 ± 0.3 and 5.2 ± 1.2 μm , respectively. (J) Time constants of calcium decay were directly proportional to terminal radius determined using imaging (grey, $n = 32$ terminals) or capacitance measurements (black, $n = 20$ terminals). The linear fit was constrained to go through the origin. Error bars show 1 standard deviation (SD). doi:10.1371/journal.pbio.1001972.g003

dynamics to predict the kinetics of vesicle release, as described in Figure 5B and below.

To model the presynaptic calcium signal, the light stimulus was convolved with the impulse response of a BC to predict the voltage trajectory in the soma (Figure 4A, top). BCs in goldfish have bandpass characteristics with peak transmission varying between about 1–14 Hz [22], and we chose a value of 9.5 Hz [29]. The voltage response in the soma was then instantaneously mapped to the presynaptic calcium current using the I–V relation and density of L-type calcium channels measured in the terminal of BCs isolated from goldfish [30]. This I–V relation is an exponential function, changing e-fold in ~ 6.6 mV over the physiological range of membrane potentials [30]. These first two steps in the model are

analogous to the linear-nonlinear (LN) model that has been used to provide a description of responses in RGCs [7]. This model therefore identifies the rectifying I–V relation of the calcium current in BCs as the first major non-linearity in retinal processing. The time-course of the presynaptic calcium signal in response to a visual stimulus was calculated by convolving the time-course of calcium influx with the “presynaptic calcium filter” predicted by the one-compartment model, which has an impulse response decaying with time-constant τ_{decay} (Figure 3E and 3F). The value of τ_{decay} depended on the radius of the terminal, according to the linear relation measured experimentally in Figure 3J.

To test this model of calcium dynamics we compared its predictions with experimental measurements made with OGB-5N

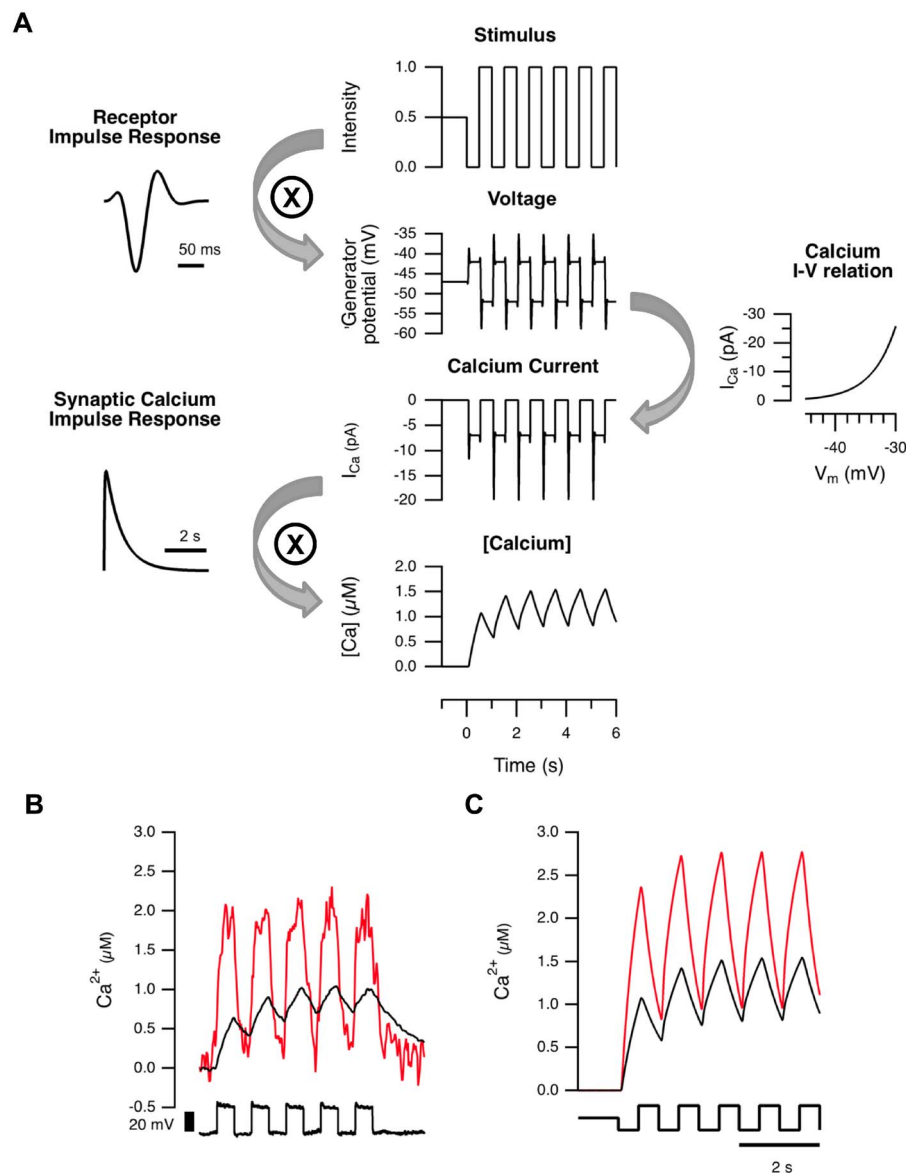


Figure 4. A simple model to predict global calcium changes in the presynaptic terminal. (A) The stimulus (here a 1 Hz square wave) was convolved with the photoreceptor impulse response to estimate membrane voltage (top). Subsequently, the current through L-type calcium channels was calculated based on the I–V relation and number of channels (middle). Convolution of the calcium current with the synaptic calcium impulse response, calculated from Figure 3G, yielded an estimate of global calcium concentration over time (bottom). (B, C) Measured (B), and modeled (C), global calcium changes in a small (red; radius = 1 μm) and large (black; radius = 3 μm) terminals responding to a 1 Hz square wave stimulus. Data in (B) from goldfish “mixed” BC (cf. Figure 3D–3J). doi:10.1371/journal.pbio.1001972.g004

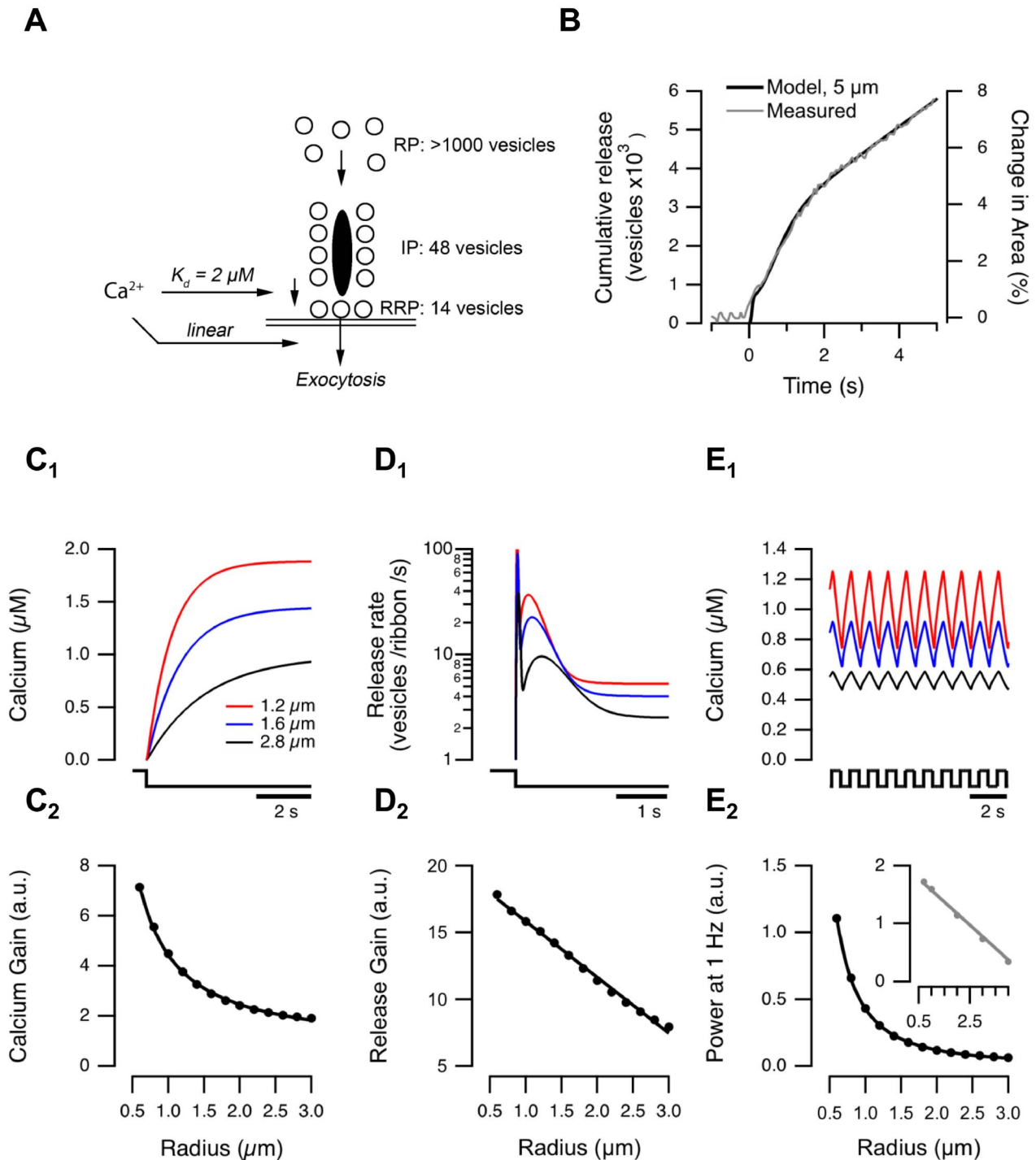


Figure 5. A model of vesicle release through the ribbon. (A) Schematic showing three vesicle pools involved in the exocytic response triggered by calcium. (B) The model (black) closely reproduces the three phases of release measured by [45] (grey) upon maximal activation of calcium channels. (C₁) Bulk calcium and (D₁) vesicle release modeled for OFF terminals with different radii (1.2, 1.6, 2.8 μm) when a light step is turned off. (C₂) The initial rate of rise of the calcium signal (calcium gain) varies as $1/r$, while release gain falls linearly with r (D₂). (E₁) Calcium in response to a 1 Hz square wave stimulus in different size terminals. (E₂) Power at the stimulus frequency falls with $1/r$ (cf. Figure 1E₂). See also Figure S4. (E₂) Inset: unlike the one-compartment model, the 3-D diffusion model (Figure S3) predicts a linear relation between power at the stimulus frequency and radius.

doi:10.1371/journal.pbio.1001972.g005

in BCs from slices of goldfish retina. The calcium concentration in the smaller of two connected synaptic compartments rose higher and faster, and then decayed almost to baseline after each cycle of a 1 Hz stimulus, while in the larger terminals there was an accumulation of calcium and much smaller modulations in concentration (Figure 4B). The model could account for these differences by using the appropriate value of r while keeping all other variables constant (Figure 4C).

We considered two extensions of this model. The first is the use of three dimensions to estimate changes in calcium concentration at the active zone: this provided a very similar prediction to the one-compartment model (Figure S3). The second extension was to add active conductances in the terminal leading to calcium spikes, but again this did not alter the main conclusions that we could draw about the impact of terminal volume on gain and kinetics (see below and Figure S6).

A Model of Synaptic Transmission through Bipolar Cells

Having established that the model accounted adequately for variations in the presynaptic calcium signal, we extended it to explore the impact of terminal size on the kinetics of vesicle release. The following properties of exocytosis at the ribbon synapse of BCs were taken into account, all of which have been measured experimentally.

Property 1. There are three anatomically distinct populations of vesicles in the synaptic terminal of BCs: the rapidly-releasable pool (RRP) docked at the active zone, the intermediate pool (IP) attached to the ribbon behind the active zone, and the reserve pool (RP) that is mobile across the whole terminal [31]. Based on the assumption of a constant ribbon density (see below), the sizes of the RRP and IP were proportional to terminal surface area, while RP size depended on volume (equation 4 in Text S1).

Property 2. There are two kinetically distinct modes of neurotransmission [32]: one is fast and transient [33] and the other slow and sustained [34].

Property 3. Both modes of exocytosis can be driven by micromolar calcium concentrations, which can be achieved in the bulk cytoplasm [34–39].

Property 4. The spatial scale on which calcium entering through calcium channels triggers exocytosis is of the order of microns. The idea that microdomains of calcium control fast release of vesicles from BCs is supported by a large number of studies demonstrating that such release is effectively blocked by the slow calcium buffer ethylene glycol tetraacetic acid (EGTA) [33,35,36,40,41].

Property 5. For simplicity we assumed that the number of ribbons, and therefore the number of L-type calcium channels, is proportional to terminal surface area. This assumption is tentatively supported by electron microscopy (EM) studies of goldfish “mixed” BCs [42].

This model closely described the different phases of exocytosis measured in isolated BCs stimulated by a voltage-clamp step (Figure 5A and 5B) [35].

To assess the utility of the model, we compared its predictions with the experimental measurements of synaptic function illustrated in Figures 1E–1G. Variations in the initial rate of rise of presynaptic calcium signal (Figure 5C_{1,2}), the initial rate of exocytosis (Figure 5D_{1,2}), and the power of the calcium signal elicited by a 1 Hz stimulus could all be accounted for by variations in terminal radius, while keeping other variables constant. For instance, the initial rate of rise of calcium in response to a step stimulus decreased as $1/r$ while the rate of exocytosis was found to decrease linearly with r *in vivo* (Figure 1E₂ and 1F₂) and the model predicted the same (Figure 5C₂ and 5D₂). A notable feature

of the model was the prediction of a secondary rise in the release rate beginning ~ 150 ms after stimulus onset. A second phase of release has also been observed experimentally by monitoring glutamate release from the BC terminal electrophysiologically in a second voltage-clamped “sniffer cell” [32].

In its simplest form, the model failed to predict the exact form of the relation between the power of the SyGCaMP2 signal and terminal radius: power varied linearly with r *in vivo* (Figure 1G₂), but the model predicted that it would vary as $1/r$ (Figure 5E₂). This discrepancy could be corrected with a 3-D diffusion model that captures local calcium differences during ongoing signaling (Figure 5E₂, inset).

We also explored predictions of the model to alterations in physiological parameters, including the possibility of a nonlinear relation between release rate and calcium concentration, and variations in the relative threshold for L-type calcium channel activation. These changes did not qualitatively alter the predicted effects of terminal volume on the gain and kinetics of signal transmission (Figure S4). The combination of experiment and modeling presented in Figures 1–5 converges on one basic idea: the volume of the presynaptic compartment is closely linked with the gain and kinetics of synaptic transmission by determining the amplitude and time-course of the presynaptic calcium transient. This fundamental property of the synaptic compartment varies across BCs (Figure 1D) and will therefore contribute to variations in the gain of the visual signal transmitted to the inner retina, as well as the way gain varies as a function of frequency.

Variations in Contrast Adaptation in Terminals of Different Volume

The gain of signal transmission through the retina is not constant, but varies continuously according to the recent history of the stimulus [8]. Such plasticity has been studied particularly intensively in the context of adaptation after an increase in temporal contrast, which involves depression of excitatory synaptic transmission from BCs to RGCs [18,43,44], likely reflecting depletion of rapidly releasable vesicles within the terminal [45–47]. Might the size of BC terminals also impact on the process of contrast adaptation? Larger BC terminals can contain hundreds of thousands of vesicles, and these are more mobile than in conventional synapses, acting to support the continuous mode of transmission [31,34]. It might therefore be expected that larger terminals containing more vesicles are more resistant to depression.

To quantify time-dependent changes in synaptic gain we used an “Adaptation Index” (AI), calculated as the ratio between the peak initial response to an increase in contrast and the later steady-state response. Using a stimulus of 100% contrast modulated at 5 Hz, and assuming a constant density of vesicles in terminals of different volume, the model predicted that the rate of vesicle release would depress more profoundly in smaller terminals (Figure 6A and 6B). This can be understood in terms the RRP and IP depleting faster and to a lower steady-state in small terminals compared to large (Figure 6A).

Assaying vesicle release *in vivo* using syHy confirmed that smaller terminals displayed greater depression (Figure 6C), and AI decreased linearly with r (Figure 6D). The absolute values of AI measured using syHy were, however, lower than those predicted by the model: in the smallest terminals, an AI of ~ 2.5 was measured using syHy, while the model predicted values of ~ 6 . This difference is likely to reflect the relatively low time-resolution of syHy measurements, causing us to underestimate the initial peak release rate (cf. Figure 6A). Nonetheless, the model and experimental measurements together demonstrate that the

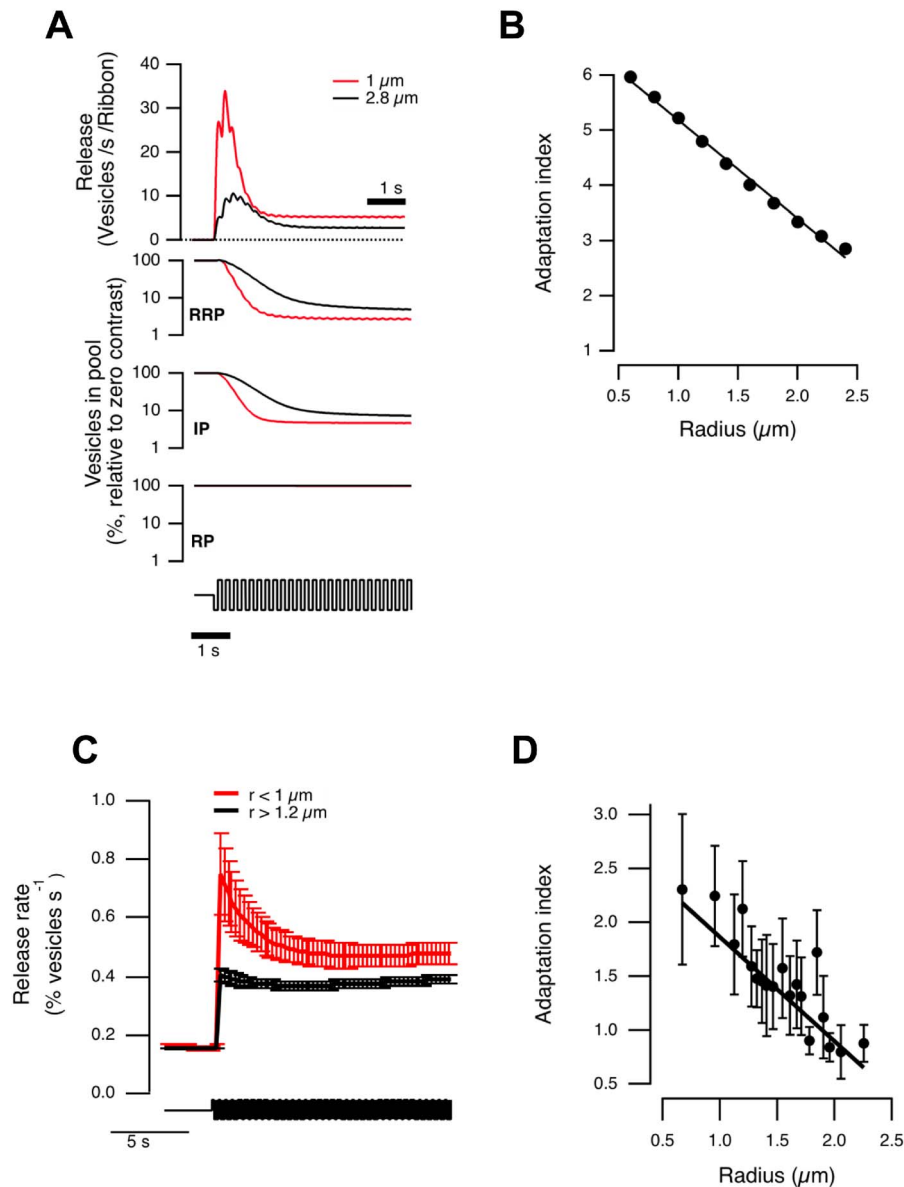


Figure 6. Contrast adaptation depends on terminal size: comparison of model and experiment. (A) Top, vesicle release modeled in small (red) and large (black) terminals in response to a 5 Hz stimulus (100% contrast). Small terminals are predicted to exhibit stronger adaptation. Bottom, dynamics of three vesicle pools used in the model. RRP and IP deplete faster in small terminals while RP in small and large terminals remains near constant. (B) Modeled adaptation index (Methods) decreases linearly with terminal radius. (C) Adaptation of synaptic output measured *in vivo* was more profound in smaller terminals. Graph shows release dynamics of OFF terminals with $r < 1 \mu\text{m}$ (red) and $r > 1.2 \mu\text{m}$ (black) in response to a 5 Hz stimulus (cf. (A)). (D) Adaptation index decreases linearly with terminal radius, as predicted by the model ($n = 236$ OFF terminals from seven fish, each bin is an average of 12 individual terminals). Spearman correlation = -0.86 , critical value ($p = 0.05$) = 0.45 . See also Figure S5. doi:10.1371/journal.pbio.1001972.g006

geometry of the presynaptic compartment is one of the factors determining the kinetics of vesicle depletion and, therefore, adaptation.

It has recently been demonstrated that there are two opposing forms of plasticity when the retina responds to an increase in temporal contrast: while some BCs and ganglion cells adapt, others become sensitized [18,48]. The balance between adaptation and sensitization was also found to vary as a function of terminal size [14,18]; on average, larger terminals tended to show less adaptation (Figure 6C) with the largest terminals exhibiting

sensitization (Figure 6D). Sensitization of the BC output has been shown to result from reduced inhibition from amacrine cells [18,19,49], and so is not predicted by the simple one compartment model.

Linear- and Non-linear Transformations of the Visual Signal: Impact of Terminal Volume

An empirical description of the relation between variations in the intensity of light falling on the retina and the spike-rate of ganglion cells can often be obtained using a model comprised of

two stages: a linear transformation of the input feeding into a rectifying non-linearity [7,50,51]. How does this linear-nonlinear (LN) model map onto the retinal circuit [5]? Transformations of the visual input are roughly linear through the processes of phototransduction and transmission by the synapses of photoreceptors, as far down the visual pathway as the cell body of BCs [22,43,52,53]. But what of the next neural compartment in the visual pathway—the synaptic terminal of BCs?

Measurements of vesicle release with synHy demonstrated strong rectification in the synaptic output because an increase in stimulus variance caused an increase in the mean rate of vesicle release even when the mean luminance was held constant, as shown in Figure 6C. This behavior is predicted by the model (Figure 6A), where it reflects the rectifying relation between membrane potential and the amplitude of the calcium current (Figure 4). To test this explanation by experiment, we imaged the presynaptic calcium signal using SyGCaMP2, while applying a square wave stimulus modulated at 3 Hz. Figure 7A compares the SyGCaMP2 signal averaged over two populations of terminals that generated a significant response to this stimulus: 66 with $r < 1.5 \mu\text{m}$ and 119 with $r > 2.5 \mu\text{m}$. In both populations the presynaptic calcium signal was a strongly rectifying function of light intensity, causing a steady increase in calcium that was graded with contrast (Figure 7B). These measurements identify voltage-dependent calcium channels in the synaptic terminal of BCs as being responsible for the first major non-linear transformation of the visual signal as it is transmitted through the retina.

Although the most obvious aspect of the SyGCaMP2 signal elicited by an increase in the variance of the stimulus was a maintained increase in presynaptic calcium, smaller fluctuations could also be detected (Figure 1G). The power of the fluctuations following a periodic stimulus was used to quantify the linear component of the synaptic calcium response [22], and the power of this linear component was ~ 3 -fold larger in the smaller population of terminals (Figures 1G, 7C, and 7D). Further, when the contrast of the stimulus was varied between 10% and 100%, the power of the linear component was directly proportional to the power of the DC component (Figure 7E), as predicted by the model (Figure 7G). The proportionality constant for the small population of terminals was 2.4 times that of the large population (Figure 7E), which was also predicted by the model. The relatively slow response time of SyGCaMP2 ($\tau_{\text{decay}} \sim 200 \text{ ms}$ [13]) prevented the imaging of synaptic responses following stimuli at frequencies greater than 3 Hz, but the results in Figure 7 demonstrate that smaller terminals generate relatively stronger linear responses than large terminals, and therefore encode fluctuating stimuli more effectively.

Variations in Temporal Filtering in Terminals of Different Volume

How do variations in filtering of the presynaptic calcium signal impact on the output from the synapse? Assaying vesicle release with synHy demonstrated that smaller terminals respond to a step of light with higher relative release rates (Figure 1F), but the resolution of this reporter was too low to detect modulations at stimulus frequencies $> 1 \text{ Hz}$ (i.e., the linear component of the output). Nonetheless, the model predicted that the modulation in release rate would be directly proportional to the steady rate once the terminal had adapted (Figure 7F), and synHy can be used to assess variations in the steady-rate of release [14]. We therefore used steady-state measurements to compare temporal filtering in the output of small and large terminals.

Figure 8A shows averaged synHy signals to stimuli of varying frequency, for two populations of terminals: small ($r < 1 \mu\text{m}$) and

large ($r > 1.5 \mu\text{m}$). The amplitude of the response, reflecting the steady rate of vesicle release, is plotted as a function of frequency in Figure 8B. Small terminals transmitted frequencies between 5 and 10 Hz significantly better than large terminals. For instance, at a frequency of 8 Hz, the relative response of small terminals was ~ 2.4 -fold that of large.

If the power of the modulated response is proportional to the mean release rate, as suggested by the results in Figure 7E, these measurements can be considered an approximation of the “transfer function” of the visual system up to the point that BCs transmit the visual signal. We therefore described the measurements using an expression commonly used to describe the output of electrical circuits with some element of resonance [54]:

$$\frac{A}{\sqrt{\left(1 - \left(f/f_0\right)^2\right)^2 + 1/Q^2 \left(f/f_0\right)^2}}$$

where A is a scaling factor, f_0 is the center frequency, and Q is a quality factor describing how much the response is damped. In small terminals, Q was estimated as 1.57 ± 0.37 , while in large terminals it was 0.78 ± 0.17 . Thus small terminals more obviously maintained the bandpass characteristics of the voltage signal measured in the cell body of BCs [22], while large terminals damped out the resonant frequencies. This behavior can now be understood in terms of the impact of terminal volume on the dynamics of the calcium signal controlling neurotransmitter release.

Discussion

Many BCs transmit the visual signal through multiple terminals located in different strata of the IPL (Figure 1). Using a combination of *in vivo* imaging, slice electrophysiology, and modeling, we have found that variations in the size of these terminals will cause the signal in a single neuron to be transformed through different temporal filters as it is transmitted to the inner retina (Figures 1–4). The mechanistic link is the calcium signal that controls synaptic transmission: smaller terminals generate larger and faster calcium transients (Figures 1–5), increasing the gain of synaptic transmission and allowing higher frequencies to be transmitted (Figures 7 and 8). Diversity in the properties of synaptic transmission extend to time-dependent changes in gain: smaller terminals adapt more completely after an increase in stimulus contrast (Figure 6). These variations in synaptic properties will expand the number of processing channels that can operate in parallel through the limited number of neurons packed into a given region of the retinal network [55,56]. These results complement recent evidence for divergence of visual channels through individual BCs, obtained by direct electrical stimulation of these neurons while monitoring the effects in multiple ganglion cells [4,11,57].

Different Temporal Channels through Individual Bipolar Cells

The different temporal channels in the visual system were first distinguished by recording responses of “transient” and “sustained” ganglion cells in the retina [4]. These temporal channels partly reflect processing in the inner retina, where feedback inhibition and lateral inhibition from amacrine cells act directly on BC terminals to alter the gain and timing of the synaptic output [11,19,58]. Here we have described a fundamental and intrinsic property that will contribute further to the diversity of signals that BCs transmit—the geometry of the synaptic compartment [11,55,56].

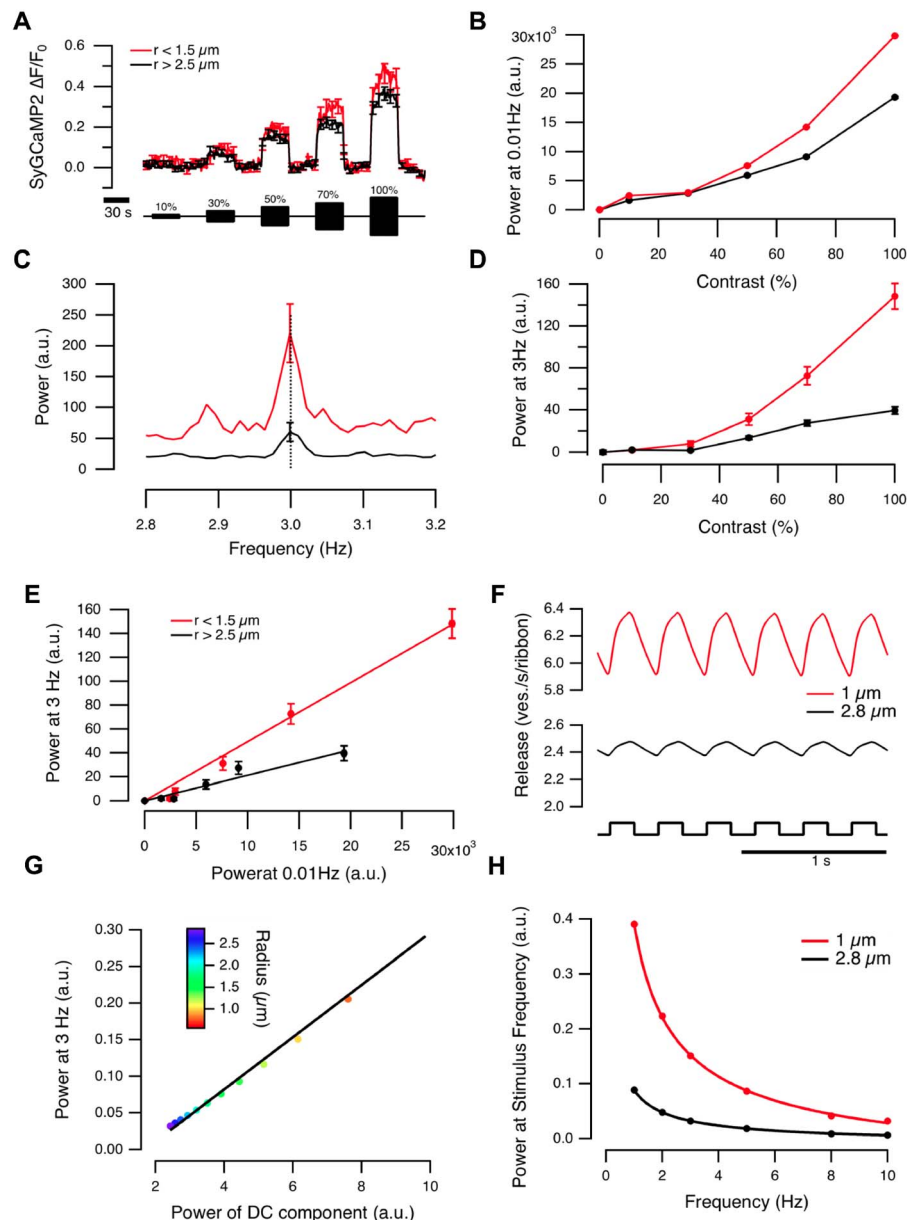


Figure 7. Linear and rectifying components of contrast response vary with terminal size. (A) SyGCaMP2 responses of BC terminals to stimuli of varying contrast (3 Hz). Average $\Delta F/F_0$ of all contrast responding terminals (both ON and OFF) with $r < 1.5 \mu m$ ($n = 66$ terminals, red) and $r > 2.5 \mu m$ ($n = 119$ terminals, black). Note how these synaptic calcium responses are strongly rectifying. (B) Power of the DC component measured at 0.01 Hz for stimuli shown in (A). The DC component was larger in small terminals (cf. Figure 4C). (C) Power spectrum of the response to 100% contrast (3 Hz) for small (red) and large (black) terminals. (D) Power at 3 Hz varies with contrast. See also Figure S4. (E) Power of the linear and DC components are directly proportional, but the proportionality coefficient is larger for smaller terminals. The Pearson correlation coefficient was 0.99 for small terminals and 0.97 for large. (F) Modeled release in response to a 3 Hz stimulus (100% contrast). (G) The model predicts that the power of the calcium response at 3 Hz is directly proportional to the power of the DC component, as was observed experimentally in (E). (H) Power of the exocytic response modeled for a range of stimulus frequencies. Power at the stimulus frequency varies as $1/f$ for both small and large terminals. doi:10.1371/journal.pbio.1001972.g007

In the future, it will be important to assess the extent to which RGCs tuned to different frequencies receive inputs from BC terminals of different sizes. Such a study will be technically demanding, requiring a detailed anatomical reconstruction of IPL circuitry. Nonetheless, Figure 1D provides the first evidence that RGCs with dendrites in different layers of the IPL will, on average, receive excitatory input from BC terminals of different

sizes. For instance, layer 6 of the IPL contains the highest density of large terminals, which leads to the testable prediction that RGCs extending dendrites in this layer will be more likely to exhibit low-pass characteristics. In contrast, layer 5 has smaller terminals than the average, suggesting that RGCs collecting inputs from this layer will be tuned to higher frequencies.

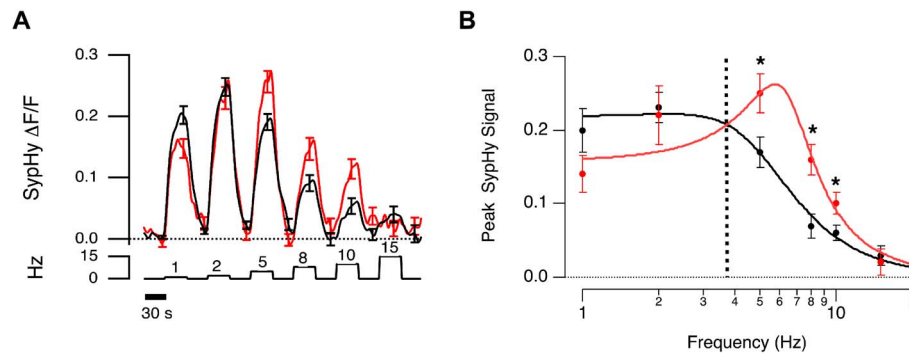


Figure 8. Frequency tuning of BCs with different terminal size. (A) Mean sybHy fluorescence signals in OFF terminals in response to full-field stimuli of different temporal frequencies measured *in vivo* (red, $r_{\text{small}} < 1 \mu\text{m}$, $n = 10$; black, $r_{\text{large}} > 1.5 \mu\text{m}$, $n = 32$). (B) Synaptic gain of large (black) and small (red) terminals as a function of stimulus frequency. Results are described by the function

$$\frac{A}{\sqrt{\left(1 - \left(f/f_0\right)^2\right) + 1/Q^2 \left(f/f_0\right)^2}}$$

For large terminals, $A = 0.22 \pm 0.02$, $f_0 = 4.96 \pm 0.45$, $Q = 0.78 \pm 0.17$. For small terminals $A = 0.16 \pm 0.02$, $f_0 = 6.43 \pm 0.27$, $Q = 1.57 \pm 0.37$. Asterisks mark significantly different responses at a given frequency, as evaluated by Mann-Whitney U test ($p < 0.05$).
doi:10.1371/journal.pbio.1001972.g008

Extrinsic Factors Affecting the Frequency Response of Bipolar Cell Synapses

The purpose of the model we have presented is to provide a basic mechanistic understanding for the impact of terminal volume on calcium dynamics and vesicle release from BCs. A more comprehensive model of signal transmission from BCs would not treat the neuron in isolation but would also consider the local circuits into which the terminals are connected. In particular we have neglected the effects of direct inhibitory feedback from amacrine cells [11,19,58]. It is, however, notable that when the GABAergic component of this feedback was blocked, the size-dependence of release rate was maintained (Figure 2), indicating that negative feedback was not the cause of this correlation.

The temporal tuning of BCs also reflects processes in the outer retina, especially cone [59] inputs with different contact morphologies acting on dendritic glutamate receptors with different kinetics of recovery from desensitization [3,60,61]. The general picture that emerges is one in which amacrine cells modulate transmission of different frequency components in the visual input by acting on the background of at least two intrinsic properties varying between BCs: tuning of dendritic inputs summed at the cell body and the filter determining calcium dynamics in the synaptic terminal providing the output (Figure 3G) [62]. The key new idea that we propose here is that this synaptic filter varies between different outputs because of variations in an intrinsic property of the synaptic compartment—its volume.

The Synaptic Compartment of Bipolar Cells as a Computational Unit

It has long been recognized that the visual system separates signals encoding different aspects of a stimulus for transmission through different pathways or “channels.” The most fundamental of these parallel representations is the separation of ON and OFF signals, which begins in distinct types of BC [63]. The separation of signals with different speeds into transient and sustained pathways also begins in BCs [6]. More than ten types of

morphologically distinct BCs can be recognized in the vertebrate retina, and probably more than 20 in zebrafish [64,65], but we still do not fully understand how these differ in their response properties. The general thinking has been that one type of BC transmits one type of signal, but more recent work indicates that it might be more fruitful to focus on the synaptic terminal as the fundamental unit of signal transmission, which would allow for divergence of different signals from the one neuron [11].

Implicit in this idea is the notion that the different synaptic outputs of a neuron are functionally isolated from each other, at least to some extent. Does the geometry of the terminal arborization allow this? Simultaneous measurements of calcium signals in connected terminals demonstrate that the answer is yes: connecting processes provide a sufficient diffusional barrier to allow calcium signals with different amplitudes and kinetics to remain local to individual terminals (Figure 3). Such isolation of presynaptic calcium signals would also allow for independent modulation of different synaptic compartments by amacrine cells. The potential number and diversity of these synaptic transformations becomes even greater if one considers that individual amacrine cells provide negative feedback through many neurites with distinct biophysical and synaptic properties [66]. Such presynaptic heterogeneity has previously been observed in sensory pathways of insects, including cricket auditory afferents [67] and *Drosophila* olfactory receptor neurons [68].

Materials and Methods

In Vivo Imaging of Presynaptic Ca^{2+} Signals and Vesicle Fusion

All procedures were carried out according to the UK Animals (Scientific Procedures) Act 1986 and approved by the UK Home Office. Transgenic zebrafish expressing SyGCaMP2.0 and sybHy were maintained on a 14/10 h light/dark cycle at 28°C. From 24 hpf the larvae were maintained in fish medium (E2) containing 1-phenyl-2-thiourea at a final concentration of 200 μM (Sigma) to prevent pigment formation. Fish were imaged as described

previously [13]. Briefly, before experiments 8–10 dpf larvae were anesthetized in 0.016% Tricaine (Sigma) and immobilized in low melting point agarose. To prevent eye movement α -bungarotoxin (2 mg/ml) was injected into the extraocular space. Imaging was performed using a custom-built multiphoton microscope, equipped with a mode-locked Chameleon titanium-sapphire laser (Coherent) tuned to 920 nm and controlled using ScanImage v.3.6 software [69].

The retina was imaged through an Olympus LUMPlanFI 40 \times water immersion (0.8 NA) objective. Green emission from syHy and SyGCaMP2 was collected both through the objective and through an oil condenser (ND 1.4, Olympus), filtered through GFP filters (530/50 nm, Chroma Technology), and detected with GaAsP photomultipliers (Hamamatsu). Images (128 \times 128 pixels) were acquired every 0.128 seconds, resulting in a sampling frequency of 7.8 Hz. Full-field light stimuli were delivered using an amber LED (590 nm) filtered through a 600/10 BP filter and projected through a light guide onto the surface of the bath, close to the eye of the fish. The mean intensity of light stimuli was $\sim 2 \times 10^5$ photons/ $\mu\text{m}^2/\text{s}$, which is in the low photopic range.

Importantly, optical measurements in the live retina necessarily give rise to a background activation of photoreceptors. This is due to direct laser activation of photopigment, but usually more importantly, due to indirect activation of photopigments from the emission light of excited fluorophores [70]. As a result, rods are typically saturated, and cones partially adapted, giving rise to a low-photopic background light-level. Indeed, we observed similar effects in our *in vivo* experiments (Figure S1F). However, this background illumination was weaker than typically observed in e.g., rabbit [70], presumably as the zebrafish retina is cone dominated. Nevertheless, following activation of the laser scanning, we typically waited 30 seconds before commencing with additional visual stimulation to ensure the retina adapted to the background levels attributed to the laser.

Image Analysis

Movies were processed using the SARFIA suite of analysis routines [17] running in Igor Pro 6 (WaveMetrics). We detected terminals on the basis of single images obtained by averaging many frames of the movie corresponding to total integration times of several tens of seconds. ROIs corresponding to terminals within these averaged images were defined using a filtering algorithm based on a Laplace operator followed by application of a threshold, as described in detail in [17]. This algorithm will define most or all of the ROIs that an experienced observer would recognize by eye. To prevent bias between ON and OFF terminals within a single field of view, the average image was obtained from movies in which light steps were applied, and/or light intensity modulated at 1 Hz or faster.

Estimation of Terminals Size by Two-Photon Imaging

The point-spread function of the used microscope in XY dimension was 0.5 μm and terminals appeared larger when we increased intensity of the 2-photon laser. We therefore tested whether terminals might appear smaller when less active, but found that this was not the case (as described in Figure S1 and Text S1). Average terminal sizes were similar between different fish (Figure S5A) and the effects of terminal size on adaptation kinetics could be observed in individual fish (Figure S5B) as well as in data averaged over multiple fish (Figure 6C). However, the distribution of estimated terminal sizes in SyGCaMP2 was shifted to larger values, compared to syHy or Synaptophysin-EGFP fish (Figure S1H). This is likely explained by the greater overall brightness of SyGCaMP2. The z-resolution of the microscope was

$\sim 2 \mu\text{m}$. Given an average radius of just above 1 micron per terminal, this resolution was therefore large enough to avoid underestimating the size of terminals traversed non-centrally by the optical plane, but small enough to avoid out-of-focus terminals contributing to the signal.

Statistical Analysis

All statistical analysis was performed in Igor Pro 7 (WaveMetrics). Differences in different parameters in large and small terminals, described in Figure 3, were analyzed using Wilcoxon signed-rank test. This test was chosen because some responses of large and small terminals were recorded from the same neuron. Sample sizes were not determined a priori. Analysis of the response dynamic was automatic and no knowledge of terminal size was used until the last moment. All animals demonstrating robust response to light were included in the analysis. Figure 1B represents biological replicate, representative from more than five fields of view. No lack of reproducibility was found. All error bars in figures show ± 1 SEM, unless stated otherwise in the legend.

Calculation of Vesicle Release Rates

V'_{exo} , the fraction of total vesicles in the terminal released per second, was calculated from the syHy signal according to the equation:

$$V'_{\text{exo}}(t) = \frac{1}{19F_{\text{min}}} \left[\frac{dF}{dt} + k_{\text{endo}}(F - F_{\text{min}}) \right] \quad (1)$$

where F is the average fluorescence intensity over the terminal at time t , F_{min} is the intensity when the rate of vesicle release is at a minimum, and k_{endo} is the rate-constant of vesicle retrieval. The calculation of this formula is described in [14,18]. Estimation of V'_{exo} requires differentiation of the syHy trace, which in turn amplifies noise, so Equation 1 was applied after smoothing with a series of single or double exponential functions to obtain “non-noisy” traces before calculation of V'_{exo} . These fits are shown in Figures 1F and 5C.

Slice Electrophysiology and Imaging

Slices of goldfish retina were perfused with extracellular solution containing (in mM) 120 NaCl, 2.5 CaCl_2 , 2 KCl, 1 MgCl_2 , 0.1 CaCl_2 , 4 HEPES, 10 glucose (pH 7.7, 255 mOsm). Experiments were carried out at room temperature and slices visualized under oblique infrared illumination through a 60 \times objective (NA 0.9) on an upright microscope. Whole cell recordings were obtained from “large” terminals (diameter: 4–12 μm) or from the soma of “mixed” BCs using 8–12 M Ω patch electrodes [71]. For this, we targeted large terminals in layers 5/6. The intracellular solution contained (in mM) 104 Kgluconate, 8 KCl, 2 MgCl_2 , 4 HEPES, 0.5 EGTA, 2 MgATP, 1 NaGTP, 1 NacGMP (pH 7.4, 250 Osm), and 100 μM of the hexapotassium salt of the low affinity Ca^{2+} indicator OGB-5N. Recordings were left for 1–5 min to allow time for the Ca^{2+} -indicator to diffuse into adjacent small terminals (diameter 1–4 μm) see also [20]. Series resistance ranged from 8–15 M Ω while input resistance was > 1 G Ω at -70 mV. Recordings were corrected for junction potentials (calculated as -11.95 mV).

OGB-5N was imaged at 40 Hz using an electron multiplying charge coupled device (EM CCD) camera (Hamamatsu C9100). Subsequent image analysis was performed using ImageJ, Igor Pro, and Matlab. OGB-5N signals were quantified as changes in fluorescence relative to background fluorescence at each pixel ($\Delta F/F_0$) and converted to estimates of absolute Ca^{2+} concentration:

$$[Ca^{2+}] = Kd \cdot \frac{F - F_{\min}}{F_{\max} - F} \quad (2)$$

F_{\max}/F_{\min} of OGB-5N is ~ 14.7 . Since resting Ca^{2+} in bipolar terminals (~ 50 nM [30]) is much lower than the K_d of OGB-5N (20 μ M) we assumed that $F_{\text{rest}} = F_{\min}$.

Supporting Information

Figure S1 Size estimation does not depend on the stimulus condition (related to Figure 1). (A) Two images of the same field of view: the left obtained from an average of 45 s in the dark, and the right averaged over a 45 s period in which the mean light intensity was in the low photopic range, including 45 s of temporal contrast applied at 1 Hz (100% contrast). Scale bar 10 μ m. (B) OFF terminals have brightest fluorescence during contrast presentation and dimmest fluorescence when exposed to steady light. Black bars show parts of the movie used for image averaging. (C) Distribution of terminal sizes estimated from averages shown in (A) (at steady light, red and temporal contrast, black). (D) Cumulative distributions, calculated from (C). (E) Terminal sizes estimated from terminals during steady and flickering light stimulation (c.f. (A)). Each point represents size estimation of an individual terminal. All points are scattered around a line through the origin with slope of 1, suggesting that size estimation is not affected significantly by the terminal activity. (F) Example of $n = 589$ OFF cells responding to laser and visual stimulation (arrows). Top: average of all responses, bottom: individual responses. Error in (standard error of the mean) SEM. (G) Responses of OFF terminals of different sizes to light decrement. Bins are the same as in Figure 1E. (I) Distributions of terminal radii calculated from individual layers. (TIF)

Figure S2 Recording “mixed” BCs from the soma (related to Figure 2). To ensure that the size dependence of current evoked calcium signals measured in different terminals belonging to the same “mixed” BC was not dependent on the position of the micropipette, we repeated experiments shown in Figure 2D–2F but this time targeted the soma of individual cells rather than the large terminal. The size dependence persisted in somatal recordings. One example of $n = 4$ is shown (c.f. Figure 2D–2F). (TIF)

Figure S3 A 3-D diffusion model of Ca^{2+} in the bipolar cell synapse (related to Figure 3). (A–C) Predicted calcium levels at different distances from a hotspot in a 5 μ m (black) and a 1 μ m (red) radius spherical compartment, shown at three different time-scales. (D) Estimated release rates driven by calcium as shown in (C). (E) Concentration of unbound “fixed” (grey) and “diffusible” (green) buffers under normal buffering conditions during step depolarisation of a 1 micron radius terminal (c.f. red in (B)). The dotted line indicates unbound buffer concentration at the channel mouth (“hotspot”), which the solid line indicates concentration at the center of the compartment. The coloration indicates the possible range of unbound buffer concentration at different locations within the compartment. (F) Corresponding calcium concentration at the hotspot (dotted) and globally (solid). (G, H) as (E, F) but with 10 times elevated “fixed” buffer concentration. Elevating the fixed buffer has only small effects on the kinetics of calcium free calcium concentration, but does affect peak calcium concentration at the hotspot. (TIF)

Figure S4 Modulation of release with changed ICa threshold and calcium dependence of release: predictions of the model (related to Figure 4). (A, B, left) Modeled calcium (A) and release (B) in response to a 3 Hz flickering stimulus from an $r = 1$ micron compartment with different thresholds for activation of the L-type calcium current (V_{rest} always = -44 mV). The threshold was increased (light green) and decreased (dark green) from the value used in the main model (red) by 3 mV in each case. Right: modulation amplitude of calcium (A) and release (B) quantified for the three threshold conditions in different size compartments. Changing the threshold had only minimal effect on the overall size dependence of calcium and release modulation. (C, D) Steady state modulation of modeled calcium (C) and release (D) in an $r = 1$ micron compartment in response to an ongoing 3 Hz stimulus. Changing the Hill coefficient for calcium dependence of release from 1 (linear = in main model, red) to 3 (cooperative, light blue) systematically increases the modulation amplitude of release (D, left) across all frequencies tested (D, right). (TIF)

Figure S5 Comparison of terminal sizes and adaptation dynamics in different fish (related to Figure 5). (A) Average terminal sizes were similar in each of six different fish. (B) Adaptation to temporal contrast (100%, 5 Hz) in a single fish. Smaller terminals (red) respond with higher gain and adapt more profoundly than large (black), in a manner similar to the behavior averaged over 6 fish (Figure 5C). (C) Same as Figure 5C, but on a longer time scale. Contrast facilitation is more pronounced in larger terminals. (TIF)

Figure S6 Active voltage spikes should boost high frequency components (related to Figure 6). (A) A “chirp” stimulus modulating at 100% contrast ramping from 0.1 to 20 Hz and back down again over a period of 10 s (top) was convolved with the same impulse response used in Figure 3 to yield a prediction of the generator potential. (B) Addition of Brownian motion noise (standard deviation [SD] = 1.4 mV) was used to yield an estimate of membrane voltage. Two separate predictions were drawn from the model at this point: graded (black) and spiking (red). A threshold was added to the “membrane voltage” trace to predict spikes, which occurred with an exponential refractory period of 300 ms. Spike amplitude was fixed at 20 mV, with a half width of 3 ms. (C) Bulk calcium and (D) release was calculated as before (Figure 4) from the graded and spiking voltage traces. (E) Average release rates of 100 graded (black) and 100 spiking (red) model BCs. Note that the mean frequency response of the spiking system is highly reminiscent of the generator frequency response (A), while the graded system imposes a powerful low pass filter on the signal. (TIF)

Table S1 List of parameters used in single compartment model. (DOCX)

Table S2 List of parameters used in 3-D model. (DOCX)

Data S1 All raw data files as well as averages and statistical parameters presented in the manuscript. Formats provided include raw-text (Ascii) and Excel (xls). In addition, we provide the original Igor-Pro files (Wavemetrics), which contain both the raw data and the original figure formatting. Data referring to particular panels are located in the

respective folders. For any further information, please contact Tom Baden at thomas.baden@uni-tuebingen.de. (ZIP)

Text S1 Supplemental information. (1) Variations in estimates of terminal size were not correlated with variations in terminal brightness. (2) Modeling presynaptic calcium dynamics and vesicle release. (3) A 3-D model predicting calcium spread at the channel mouth. (4) The effect of changing L-type calcium channel threshold and calcium dependency of release: predictions of the model. (5) Encoding of high frequency components using spikes. (6) Supplemental references. (DOCX)

References

- Masland RH (2001) The fundamental plan of the retina. *Nat Neurosci* 4: 877–886.
- Roska B, Werblin F (2001) Vertical interactions across ten parallel, stacked representations in the mammalian retina. *Nature* 410: 583–587.
- Wässle H (2004) Parallel processing in the mammalian retina. *Nat Rev Neurosci* 5: 747–757.
- Masland RH (2012) The neuronal organization of the retina. *Neuron* 76: 266–280.
- Euler T, Haverkamp S, Schubert T, Baden T (2014). Retinal bipolar cells: elementary building blocks of vision. *Nat Rev Neurosci* 15: 507–519.
- Awatramani GB, Slaughter MM (2000) Origin of transient and sustained responses in ganglion cells of the retina. *J Neurosci* 20: 7087–7095.
- Gollisch T, Meister M (2010) Eye smarter than scientists believed: neural computations in circuits of the retina. *Neuron* 65: 150–164.
- Hosoya T, Baccus SA, Meister M (2005) Dynamic predictive coding by the retina. *Nature* 436: 71–77.
- Taylor W, Smith R (2011) Trigger features and excitation in the retina. *Curr Opin Neurobiol* 21: 672–678.
- Abbott LF, Regehr WG (2004) Synaptic computation. *Nature* 431: 796–803.
- Asari H, Meister M (2012) Divergence of visual channels in the inner retina. *Nat Neurosci* 15: 1581–1589.
- Mintz I, Sabatini B, Regehr W (1995) Calcium control of transmitter release at a cerebellar synapse. *Neuron* 15: 675–688.
- Dreosti E, Odermatt B, Dorostkar M, Lagnado L (2009) A genetically encoded reporter of synaptic activity in vivo. *Nat Methods* 6: 883–889.
- Odermatt B, Nikolaev A, Lagnado L (2012) Encoding of luminance and contrast by linear and nonlinear synapses in the retina. *Neuron* 73: 758–773.
- Granseth B, Odermatt B, Royle SJ, Lagnado L (2006) Clathrin-mediated endocytosis is the dominant mechanism of vesicle retrieval at hippocampal synapses. *Neuron* 51: 773–786.
- Dreosti E, Esposti F, Baden T, Lagnado L (2011) In vivo evidence that retinal bipolar cells generate spikes modulated by light. *Nat Neurosci* 14: 951–952.
- Dorostkar MM, Dreosti E, Odermatt B, Lagnado L (2010) Computational processing of optical measurements of neuronal and synaptic activity in networks. *J Neurosci Methods* 188: 141–150.
- Nikolaev A, Leung KM, Odermatt B, Lagnado L (2013) Synaptic mechanisms of adaptation and sensitization in the retina. *Nat Neurosci* 16: 934–941.
- Vigh J, Vickers E, von Gersdorff H (2011) Light-evoked lateral GABAergic inhibition at single bipolar cell synaptic terminals is driven by distinct retinal microcircuits. *J Neurosci* 31: 15884–15893.
- Kim MH, Vickers E, von Gersdorff H (2012) Patch-clamp capacitance measurements and Ca(2+)-imaging at single nerve terminals in retinal slices. *J Vis Exp* pii: 3345.
- Protti DA, Flores-Herr N, von Gersdorff H (2000) Light evokes Ca²⁺ spikes in the axon terminal of a retinal bipolar cell. *Neuron* 25: 215–227.
- Baden T, Esposti F, Nikolaev A, Lagnado L (2011) Spikes in retinal bipolar cells phase-lock to visual stimuli with millisecond precision. *Curr Biol* 21: 1859–1869.
- Saszik S, DeVries SH (2012) A mammalian retinal bipolar cell uses both graded changes in membrane voltage and all-or-nothing Na⁺ spikes to encode light. *J Neurosci* 32: 297–307.
- Lagnado L, Cervetto L, McNaughton PA (1992) Calcium homeostasis in the outer segments of retinal rods from the tiger salamander. *J Physiol* 455: 111–142.
- Sabatini BL, Oertner TG, Svoboda K (2002) The life cycle of Ca(2+) ions in dendritic spines. *Neuron* 33: 439–452.
- Crank J (1975) The mathematics of diffusion. 2nd edition. Oxford: Clarendon Press.
- Allbritton NL, Meyer T, Stryer L (1992) Range of messenger action of calcium ion and inositol 1,4,5-trisphosphate. *Science* 258: 1812–1815.
- Kim MH, Li GL, van Gersdorff H (2013) Single calcium channels and exocytosis in sensory synapses. *J Physiol* 591: 3167–3178.
- Schnapf JL, Nunn BJ, Meister M, Baylor DA (1990) Visual transduction in cones of the monkey *Macaca fascicularis*. *J Physiol* 427: 681–713.
- Burrone J, Lagnado L (1997) Electrical resonance and Ca²⁺ influx in the synaptic terminal of depolarizing bipolar cells from the goldfish retina. *J Physiol* 505: 571–584.
- Holt M, Cooke A, Neef A, Lagnado L (2004) High mobility of vesicles supports continuous exocytosis at a ribbon synapse. *Curr Biol* 14: 173–183.
- von Gersdorff H, Sakaba T, Berglund K, Tachibana M (1998) Submillisecond kinetics of glutamate release from a sensory synapse. *Neuron* 21: 1177–1188.
- Mennerick S, Matthews G (1996) Ultrafast exocytosis elicited by calcium current in synaptic terminals of retinal bipolar neurons. *Neuron* 17: 1241–1249.
- Lagnado L, Gomis A, Job C (1996) Continuous vesicle cycling in the synaptic terminal of retinal bipolar cells. *Neuron* 17: 957–967.
- Neves G, Lagnado L (1999) The kinetics of exocytosis and endocytosis in the synaptic terminal of goldfish retinal bipolar cells. *J Physiol* 515: 181–202.
- Beaumont V, Llobet A, Lagnado L (2005) Expansion of calcium microdomains regulates fast exocytosis at a ribbon synapse. *Proc Natl Acad Sci U S A* 102: 10700–10705.
- Thoreson WB, Rabl K, Townes-Anderson E, Heidelberger R (2004) A highly Ca²⁺-sensitive pool of vesicles contributes to linearity at the rod photoreceptor ribbon synapse. *Neuron* 42: 595–605.
- Jackman SL, Choi SY, Thoreson WB, Rabl K, Bartoletti TM, Kramer RH (2009) Role of the synaptic ribbon in transmitting the cone light response. *Nat Neurosci* 12: 303–310.
- Rieke F, Schwartz EA (1996) Asynchronous transmitter release: control of exocytosis and endocytosis at the salamander rod synapse. *J Physiol* 493: 1–8.
- Burrone J, Neves G, Gomis A, Cooke A, Lagnado L (2002) Endogenous calcium buffers regulate fast exocytosis in the synaptic terminal of retinal bipolar cells. *Neuron* 33: 101–112.
- Coggins M, Zenisek D (2009) Evidence that exocytosis is driven by calcium entry through multiple calcium channels in goldfish retinal bipolar cells. *J Neurophysiol* 101: 2601–2619.
- von Gersdorff H, Vardi E, Matthews G, Sterling P (1996) Evidence that vesicles on the synaptic ribbon of retinal bipolar neurons can be rapidly released. *Neuron* 16: 1221–1227.
- Baccus SA, Meister M (2002) Fast and slow contrast adaptation in retinal circuitry. *Neuron* 36: 909–919.
- Manookin MB, Demb JB (2006) Presynaptic mechanism for slow contrast adaptation in mammalian retinal ganglion cells. *Neuron* 50: 453–464.
- Burrone J, Lagnado L (2000) Synaptic depression and the kinetics of exocytosis in retinal bipolar cells. *J Neurosci* 20: 568–578.
- Jarsky T, Cembrowski M, Logan SM, Kath WL, Rieke H, et al. (2011) A synaptic mechanism for retinal adaptation to luminance and contrast. *J Neurosci* 31: 11003–11015.
- Ozuysal Y, Baccus SA (2012) Linking the computational structure of variance adaptation to biophysical mechanisms. *Neuron* 73: 1002–1015.
- Kastner DB, Baccus SA (2011) Coordinated dynamic encoding in the retina using opposing forms of plasticity. *Nat Neurosci* 14: 1317–1322.
- Li GL, Vigh J, von Gersdorff H (2007) Short-term depression at the reciprocal synapses between a retinal bipolar cell terminal and amacrine cells. *J Neurosci* 27: 7377–7385.
- Schwartz GW, Okawa H, Dunn FA, Morgan JL, Kerschensteiner D, et al. (2012) The spatial structure of a nonlinear receptive field. *Nat Neurosci* 15: 1572–1580.
- Bolinger D, Gollisch T (2012) Closed-loop measurements of iso-response stimuli reveal dynamic nonlinear stimulus integration in the retina. *Neuron* 73: 333–346.
- Rieke F (2001) Temporal contrast adaptation in salamander bipolar cells. *J Neurosci* 21: 9445–9454.
- Schwartz G, Rieke F (2011) Perspectives on: information and coding in mammalian sensory physiology: nonlinear spatial encoding by retinal ganglion cells: when 1+1 not equal 2. *J Gen Physiol* 138: 283–290.
- Wickert M (2013) Signals and systems for dummies. Hoboken (New Jersey): Wiley.

Acknowledgments

We thank Jamie Johnston for criticisms of the manuscript and all members of the lab for discussions.

Author Contributions

The author(s) have made the following declarations about their contributions: Conceived and designed the experiments: TB AN FE ED BO LL. Performed the experiments: TB AN FE ED BO. Analyzed the data: TB AN FE ED BO LL. Wrote the paper: TB AN LL.

55. Perge JA, Koch K, Miller R, Sterling P, Balasubramanian V (2009) How the optic nerve allocates space, energy capacity, and information. *J Neurosci* 29: 7917–7928.
56. Balasubramanian V, Sterling P (2009) Receptive fields and functional architecture in the retina. *J Physiol* 587: 2753–2767.
57. Mghina M, Millar AG, Charlton MP, Govind CK, Atwood HL (1999) Calcium entry related to active zones and differences in transmitter release at phasic and tonic synapses. *J Neurosci* 19: 8419–8434.
58. Baccus SA (2007) Timing and computation in inner retinal circuitry. *Annu Rev Physiol* 69: 271–290.
59. Baden T, Euler T, Weckstrom M, Lagnado L (2013) Spikes and ribbon synapses in early vision. *Trends Neurosci* 36: 480–488.
60. DeVries SH, Schwartz EA (1999) Kainate receptors mediate synaptic transmission between cones and ‘Off’ bipolar cells in a mammalian retina. *Nature* 397: 157–160.
61. DeVries SH, Li W, Saszik S (2006) Parallel processing in two transmitter microenvironments at the cone photoreceptor synapse. *Neuron* 50: 735–748.
62. Robinson J, Schmitt EA, Harosi FI, Reece RJ, Dowling JE (1993) Zebrafish ultraviolet visual pigment: absorption spectrum, sequence, and localization. *Proc Natl Acad Sci U S A* 90: 6009–6012.
63. Werblin FS, Dowling JE (1969) Organization of the retina of the mudpuppy, *Necturus maculosus*. II. Intracellular recording. *J Neurophysiol* 32: 339–355.
64. Connaughton V, Graham D, Nelson R (2004) Identification and morphological classification of horizontal, bipolar, and amacrine cells within the zebrafish retina. *J Comp Neurol* 477: 371–385.
65. Li YN, Tsujimura T, Kawamura S, Dowling JE (2012) Bipolar cell-photoreceptor connectivity in the zebrafish (*Danio rerio*) retina. *J Comp Neurol* 520: 3786–3802.
66. Grimes WN, Zhang J, Graydon CW, Kachar B, Diamond JS (2010) Retinal parallel processors: more than 100 independent microcircuits operate within a single interneuron. *Neuron* 65: 873–885.
67. Baden T, Hedwig B (2010) Primary afferent depolarization and frequency processing in auditory afferents. *J Neurosci* 30: 14862.
68. Gaudry Q, Hong EJ, Kain J, de Bivort BL, Wilson RI (2013) Asymmetric neurotransmitter release enables rapid odour lateralization in *Drosophila*. *Nature* 493: 424–428.
69. Pologruto TA, Sabatini BL, Svoboda K (2003) ScanImage: flexible software for operating laser scanning microscopes. *Biomed Eng OnLine* 2: 9.
70. Euler T, Hausselt SE, Margolis DJ, Breuninger T, Castell X, et al. (2009) Eyecup scope—optical recordings of light stimulus-evoked fluorescence signals in the retina. *Pflügers Arch* 457: 1393–1414.
71. Palmer MJ, Hull C, Vigh J, von Gersdorff H (2003) Synaptic cleft acidification and modulation of short-term depression by exocytosed protons in retinal bipolar cells. *J Neurosci* 23: 11332–11341.